Research Article | Vol. 27, No. 25 / 9 December 2019 / Optics Express 36875
Optics EXPRESS

Efficient quasi-phase-matching in fan-out PPSLT crystal waveguides by femtosecond laser direct writing

LINGQI LI,[1] CAROLINA ROMERO,[2] JAVIER R. VÁZQUEZ DE ALDANA,[2] LEI WANG,[1,*] YANG TAN,[1] AND FENG CHEN[1]

[1] School of Physics, State Key Laboratory of Crystal Materials, Shandong University, Jinan 250100, China
[2] Grupo de Investigación en Aplicaciones del Láser y Fotónica, Departamento de Física Aplicada, University of Salamanca, Salamanca 37008, Spain
[*] leiwangsdu@sdu.edu.cn

Abstract: We demonstrate second harmonic generations in quasi-phase matched cladding waveguide structures fabricated by direct femtosecond laser writing. Waveguides with circular section are inscribed in z-cut MgO doped stoichiometric lithium tantalate with fan-out $\chi^{(2)}$ grating structures. The ferroelectric domain-inverted fan-out grating period seamlessly varies from 7.5 to 8.2 μm. Seven individual waveguides with step changed periods are fabricated. The minimum insertion loss of the cladding waveguides is about 0.54 dB at wavelength of 1064 nm. Temperature tuned second harmonic generations of 1064 nm for different quasi phase matched grating periods are demonstrated by using continuous wave and pulsed laser. A comparable normalized conversion efficiency of 3.55%/(W·cm^2) is obtained for 7.91 μm period. The maximum power conversion efficiency of 54.3% was obtained under a pump peak power of 282 W.

1. Introduction

MgO doped stoichiometric lithium tantalate (SLT) crystals have been spotlighted as an ideal candidate for nonlinear optical processes owing to its high optical nonlinearity (d_{33}≈13pm/V) and high optical damage resistance [1,2]. MgO doped SLT shows several advantages over $LiNbO_3$, such as shorter ultraviolet cut-off wavelength down to 0.28 μm, lower coercive fields, and tiny absorption of green-induced infrared wave [3–5]. Some significant results have been achieved in SLT bulk configuration including the high-power second harmonic generation (SHG) in green spectral region, high energy level as high as 21 mJ in the pulsed regime and optical parameter generation in the near-infrared in high repetition rate [4–9]. The birefringent phase matching and quasi phase matching (QPM) is the most common methods to achieve SHG in optical crystals. Due to its weak birefringence, the birefringent phase matching is not allowed in SLT crystal. The QPM in SLT accesses the material's largest optical nonlinear coefficient d_{33}. In addition, the QPM allows one to design flexible domain-inverted grating pattern to achieve effective nonlinear conversion at various wavelength [10–13]. Nevertheless, the typical QPM devices possess a single, fixed-period domain grating pattern. This design could be limited when some applications requires seamlessly tune the wavelength over a broad and complete spectral range. Based on this requirement, the design of fan-out domain-inverted grating pattern provides an ideal and efficient way [14–15].

Optical waveguides, as the basic components in integrated photonics, could confine the light fields in a small volume tightly with a long interaction length [16]. Therefore, much higher optical intra-cavity intensities could be achieved with respect to bulk materials. Some optical properties, e.g., nonlinear response and laser performance might be enhanced [17–20]. Benefiting from the compact geometry of cross section and long interaction length, frequency conversion in nonlinear

#379591 https://doi.org/10.1364/OE.27.036875
Journal © 2019 Received 3 Oct 2019; revised 20 Nov 2019; accepted 20 Nov 2019; published 4 Dec 2019

Optics EXPRESS

waveguides structure can be realized in a much lower power level than bulk configuration. Hence, optical waveguides in nonlinear crystals have become one of the preferred choices for frequency doubling [21–25]. To fabricate waveguides in LT crystal, diverse techniques have been widely employed. Especially, annealed proton exchange is the most common-used methods [26,27]. Although this manner provides high quality waveguides, they are limited to a two-dimensional planar configuration at the device surface. Moreover, this solution requires complicated multi-step fabrication processing. Recently, femtosecond laser writing has become an efficient and flexible technique to fabricate versatile waveguides at three-dimension geometry in diverse transparent materials since the work of Davis *et al* in 1996 [28–35]. During the processing of femtosecond laser writing, permanent and stable index modification can be created in the focal volume though nonlinear processes such as tuning ionization, multiphoton absorption and avalanche ionization. As a result, this refractive index change can be used for waveguide fabrication [36]. The femtosecond laser induced negative refractive change (Δn<0) usually employed as the configuration of Type II waveguides and depressed cladding waveguides [37–40]. In order to allow efficient frequency conversion, low-loss high quality waveguides are required while keeping the large nonlinear coefficients of bulk. Thus, the geometry of depressed cladding waveguides is favorable since it consists an undamaged circular core surrounded by many tracks with low index change. In addition, it allows one to create desired cross-sectional dimension and eases to integrate with optical fibers [41–43]. In recent studies, PPSLT waveguides with three/five cladding layers are fabricated by femtosecond writing [44]. The waveguides show excellent guiding at infrared waveband with very low propagation loss. However, the fabrication process is complicated and the normalized SHG conversion efficiency is limited to 0.16%/(W·cm^2) in the high-power continuous wave (CW) regime. In our previous work, because of self-focusing in the process of femtosecond laser writing, the laser-induced tracks have multi-foci. Thus, the propagation loss is high, which leads to a deteriorated performance. The nonlinear conversion efficiency is as low as 0.74%/(W·cm^2) in low-power regime [45]. To generate high quality waveguides and efficient SHG conversion efficiency in PPSLT, further exploration of femtosecond laser witting parameter is required urgently.

In this work, we report on the quasi phase matched SHG in depressed cladding waveguides in fan-out MgO doped PPSLT crystal fabricated by femtosecond laser direct writing. The minimum insertion loss of the fabricated waveguides is about 0.54 dB at wavelength of 1064 nm. Seven circular waveguides are fabricated in different position of fan-out crystal with 30 μm diameter, corresponding to different poling period. The second harmonic characteristics at 532 nm are investigated with CW and pulsed lasers at varied fundamental peak power. In the CW laser regime, the highest nonlinear conversion efficiency is 3.55%/(W·cm^2) for 7.91 μm poled period. In the short pulsed laser regime, a comparable normalized conversion efficiency of 3.81%/(W·cm^2) is obtained at low pump power. The maximum power conversion efficiency of 54.3% was achieved, corresponding to a SHG peak power of 153 W and an incident fundamental power of 282 W.

2. Experimental details

The z-cut 1mol% MgO doped fan-out PPSLT crystal used in this work is cut into the wafer with dimensions of 0.5 (z) × 11 (x) × 7 (y) mm^3. The ferroelectric domain-inverted grating pattern is fan-out across the width of the sample with seamlessly varied poling period from 7.5 to 8.2 μm. The fabrication process of femtosecond laser direct wiring waveguides is based on a Ti:Sapphire amplified femtosecond laser system (Spitfire, Spectra Physics). The linear polarized laser pulse has a temporal duration of 120 fs, a 1 kHz repetition rate, and 1 mJ maximum pulse energy at a central wavelength of 800 nm. Figure 1(b) depicts the schematic illustration of femtosecond laser fabrication process. The laser beam is focused by a 40 × microscope objective (N.A. = 0.65) at 100 μm beneath the sample surface (11 × 7 mm^2). The explored pulse energy is reduced by a calibrated neutral density filter. The sample is hold on a PC-controlled 3D motorized stage with

Optics EXPRESS

a spatial resolution of 100 nm. Different pulse energies (ranging from 0.1 to 0.7 μJ) are tried to find the favorable pulse energy and the value of 0.22 μJ is selected to fabricate the waveguides. In order to fabricate the low-index tracks, the sample is scanned by the femtosecond laser at a constant speed of 500 μm/s along the *x*-axis (11-mm edge) while producing a damage track inside the sample. The writing procedure is repeated and 28 elliptical tracks with 3 μm lateral separation are produced at different depth to construct the circular cladding geometry. Seven depressed cladding waveguides with 30 μm diameter are fabricated at different position of the fan-out sample, corresponding to the different poling period.

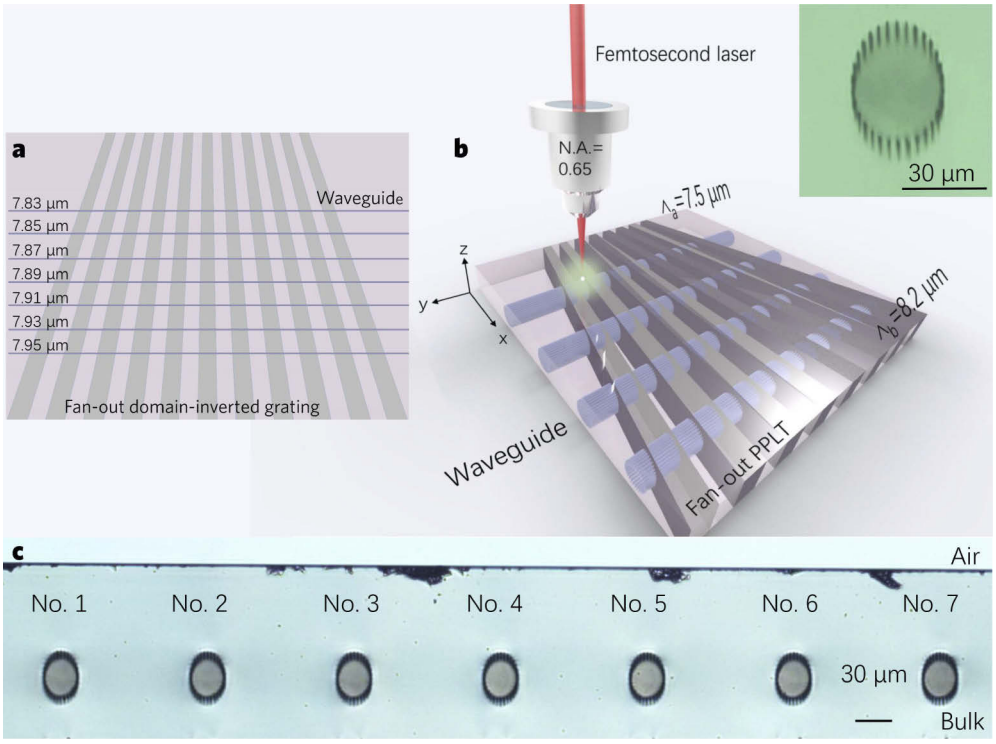

Fig. 1. The fabrication process of depressed cladding waveguides in fan-out PPSLT crystal. (a) The schematic diagram of the fan-out domain-inverted grating with pattern period seamlessly vary from 7.5 to 8.2 μm. Seven waveguides are fabricated at different position of sample, corresponding to the poling period from 7.83 to 7.95 μm with steps of 0.02 μm within the pattern. (b) Schematic plot of femtosecond laser direct writing. (c) Optical microscope cross-sectional image of waveguides No. 1 to No. 7, corresponding to 7.83 to 7.95 μm. The inset picture is the optical microscope image of waveguide No. 5.

To experimentally characterize the propagation properties of the femtosecond laser written waveguides, a typical end-face coupling system is employed to measure the propagation loss and the mode intensity profiles. An optical microscope (Axio Imager, Carl Zeiss) is used to collect the optical cross-sectional images. The propagation attenuations of seven waveguides are evaluated by direct measure the input power and output power of the transmitted laser beam. Additionally, we utilize Fabry-Pérot (FP) interference method to obtain the propagation loss around 1.55 μm. The light from a tunable semiconductor laser (TSL210VF, Santec, Japan) is butt coupled to the cladding waveguides by a polarization-maintained single mode fiber. The output power is collected by an objective lens. The wavelength tuning range is from 1260nm to 1630 nm.

Optics EXPRESS

The SHG experiments is carried out under the similar end-face coupling arrangement in the continuous-wave and pulsed laser, which is shown in Fig. 2. A linear polarized CW laser and Q-switched pulsed laser (5.2 ns, 3.62 kHz) operating at 1064 nm are implemented as fundamental laser source. The laser is along TM polarization controlled by a half-wave plate to use the largest second order nonlinear coefficient, d_{33}. The incident laser and frequency doubling laser are coupled by similar 25× objective lens. An optical low pass filter (OLPF) is employed to separate the fundamental and second harmonic laser. The power meter and CCD camera were used to characterize the power and mode profile of the out coupling light, respectively. In order to adjust the temperature of quasi-phase-matching, the sample is placed on a heating oven (Thorlabs, PV10), which could tune the temperature from room temperature to 200°C.

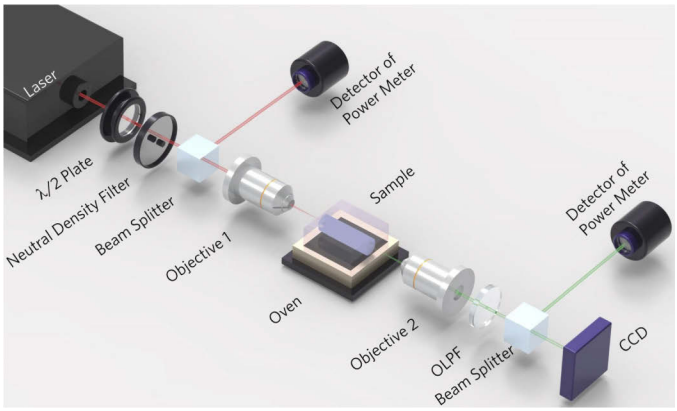

Fig. 2. Schematic plot of experimental arrangement for SHG in depressed cladding waveguides in MgO doped fan-out PPSLT crystal.

3. Results and discussion

The schematic diagram of the ferroelectric domain-inverted fan-out grating pattern and the position of waveguides array are shown in Fig. 1(a). The grating period is smoothly varied from 7.5 to 8.2 μm. Figure 1(c) depicts the optical cross-sectional microscope images of waveguides Nos. 1-7, corresponding to the poling period of 7.83, 7.85, 7.87, 7.91, 7.93 and 7.95 μm. All the waveguides have the same diameter of 30 μm. In order to fabricate low-loss and high quality waveguides, further exploration of the optimized fabrication condition in our experiments is necessary. At the previous work [45], the appearance of multi focus point induced by the self-focusing in the process of fabrication cause the irregular high order mode profiles, which could lead to big propagation loss. In this work, we decrease the focal depth to 100 μm beneath the surface. For the shallower focal depth, the spherical aberration effect can be reduced to form a more compact focalization. Self-focusing could also be prevented so than energy threshold for the track formation is lower [38]. In this work, a lower pulse energy of 0.22 uJ is used to construct a nearly perfect circular waveguide with 28 elliptical tracks, which is shown in the inset picture of Fig. 1. The insertion loss is determined by comparing the pump power of 1064 nm measured at the input/output facets while maintaining the temperature of the sample away from the phase matching temperature. The measured insertion loss results are list in Table. 1. Since the losses of Fresnel reflection of the front/rear facets (about 1.21 dB) and the objective lens transmission (about 1.22 dB) are the same for seven waveguides, both losses were excluded. All the insertion losses of seven waveguides are well below 1 dB. We note that the insertion loss contains the propagation loss and the coupling loss between the input focus spot and the waveguide mode profile, which means that both losses are satisfied for the next SHG applications.

Optics EXPRESS

Notably, minimum loss of waveguide No. 5 at 1064 nm is 0.54 dB for n_e polarization. Compared with the 2.1 dB/cm propagation loss of n_e polarization in previous work [45], the insertion loss value in our work are promoted greatly. We characterized the propagation loss of the sample further by using the Fabry-Pérot (FP) interference method. By tuning the wavelength of the transmitted laser around 1.55 μm, the propagation loss can be evaluated from the interference fringe with the following equations.

$$\alpha = \frac{4.34dB}{L}\left(\ln R - \ln\left(\frac{1-\sqrt{1-K^2}}{K}\right)\right) \tag{1}$$

$$K = \frac{I_{\max} - I_{\min}}{I_{\max} + I_{\min}} \tag{2}$$

Where L is the effective length of light propagating in the sample. R is the Fresnel reflectance. I_{max} and I_{min} are the maximum and minimum transmitted power. Table 1 lists the propagation losses of the cladding waveguides in PPSLT. The minimum loss is 1.56 dB/cm for No. 5 at 1.55 μm along n_e polarization. The interference fringes of cladding waveguide No. 5 is presented in Fig. 3(a). It is evident that the waveguides show better guiding performance under 1.064 μm compared to 1.55 μm. The larger propagation loss under 1.55 μm is induced by the tunneling loss which is more remarkable at longer wavelength.

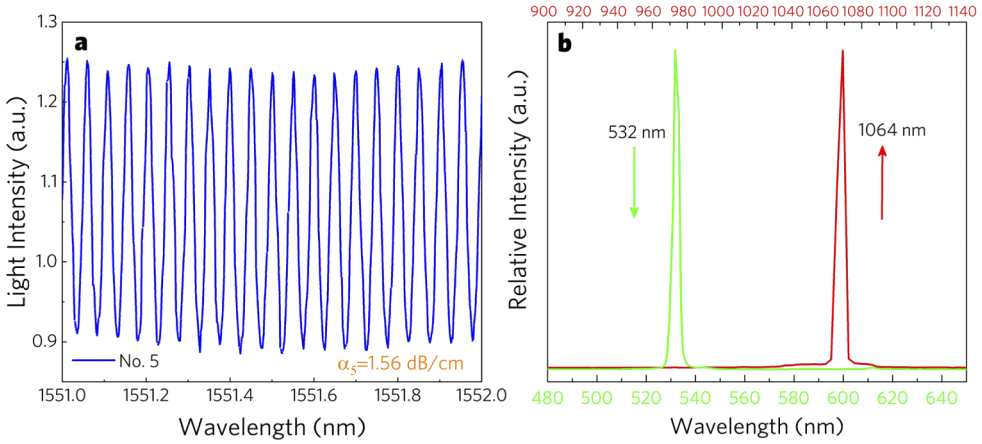

Fig. 3. (a) The FP interference fringe of the waveguide No. 5 measured by wavelength tuning. Propagation loss of waveguide No. 5 = 1.56 dB/cm at 1550 nm. (b) The spectra of the fundamental laser beam at 1064 nm and the SHG at 532 nm transmitted of MgO: PPSLT cladding waveguide.

Figure 3(b) illustrates the normalized laser spectra of the fundamental laser beam at 1064 nm (CW) and the SHG at 532 nm. By tuning the temperature of sample, QPM is realized in all seven of the cladding waveguides with different poling periods. Second harmonic power as a function of the crystal temperature is shown in the Fig. 4(a). As we can see, there is a power peak when temperature is 81.5°C, corresponding to the phase-matching temperature with the poling period of 7.91 μm. The near-field mode-profiles of second harmonic 532 nm and fundamental wave 1064 nm at the phase-matching temperature are depicted in Figs. 4(b) and 4(c). It is clearly that both mode patterns are well confined in the manner of single mode which means a good spatial overlap in the QPM process.

To demonstrate the relationship between the QPM period and corresponding temperature and to emphasize the potential applications for multi-wavelength on-chip SHG, we investigate the

Optics EXPRESS

Table 1. Propagation attenuations of depressed cladding waveguides

Waveguides	Insertion loss at 1064 nm (dB)	Propagation loss at 1550 nm (dB/cm)
	TM (n_e)	TM (n_e)
No.1	0.77	1.91
No.2	0.69	2.08
No.3	0.73	2.16
No.4	0.59	1.83
No.5	0.54	1.56
No.6	0.64	1.61
No.7	0.72	1.85

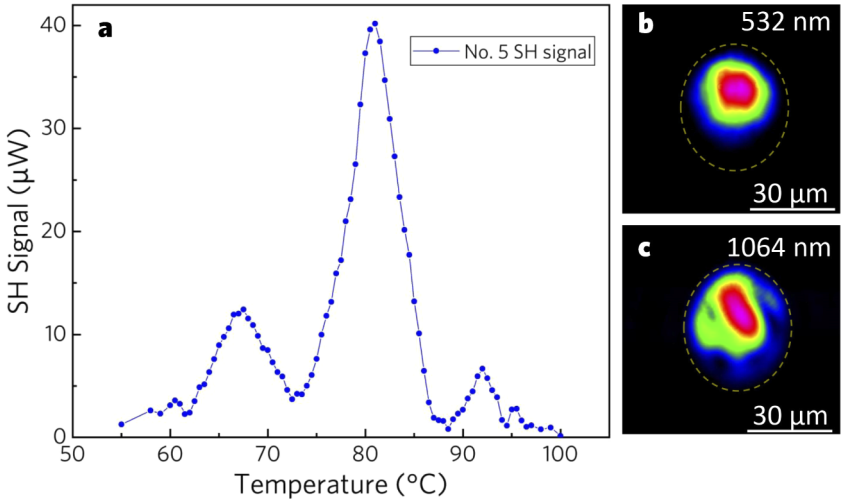

Fig. 4. (a) Experimental temperature tuning curve of SHG output power of 11 mm long PPSLT waveguide with 7.91 μm QPM period (No. 5) measured by CW laser. (b) The near-field mode-profiles of second harmonic 532 nm and (c) fundamental wave 1064 nm at the phase-matching temperature T = 81.5 °C. The yellow dotted circles in (b) and (c) are the sign of the written tracks.

SHG effect of all seven of the cladding waveguides with different period. According to the inscription geometry, the QPM period of the seven waveguides is stepwise reduced by 20 nm from 7.95 to 7.83 μm. Figure 5(a) shows the temperature dependence of the SH output power of all seven waveguides with different periods. It can be clearly seen that the waveguides with different poling periods have different QPM temperature, in which the SH power would reach its maximum. We plot the relationship between the periods of seven waveguides (Nos. 1-7) and the corresponding QPM temperature. Accordingly, the QPM temperature shifts by 10°C while changing the period per 20 nm of waveguides Nos. 1-7. A shorter QPM period corresponds to a higher QPM temperature. We have also depicted the QPM temperatures of different periods of bulk materials in Fig. 5(b). Notably, in the same poling period, the QPM temperature of waveguide is lower than bulk material, which could attribute to the dispersion deviation of the cladding waveguide structure compared to the bulk material.

We then keep each waveguide at their exact QPM temperature to measure the second harmonic power at 532 nm while the incident fundamental power is varied. Figure 6(a) depicts the dependence of SH power and normalized conversion efficiency on the incident fundamental

Optics EXPRESS

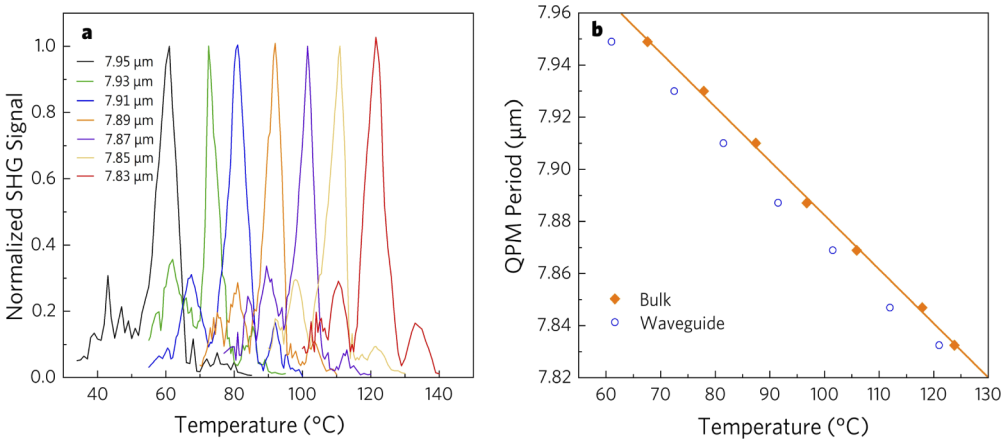

Fig. 5. (a) Normalized temperature tuning curve of all seven waveguides with different periods, corresponding to different QPM temperature. (b) The calculated QPM temperatures corresponding to different periods of bulk materials (yellow line) at wavelength of 1064 nm. The seven blue circles denote the QPM temperatures of the seven cladding waveguides (Nos.1-7).

power of the waveguide No. 5 with the 7.91 μm poling period at the CW laser regime. The SH power follows the quadratic law in the CW laser. In the low conversion efficiency regime where the depletion of fundamental wave can be ignored, the normalized conversion efficiency can be evaluated by the following equation:

$$\eta = \frac{P_{2\omega}}{(L \cdot P_{\omega}^{in})^2} = \frac{8\pi^2 d_{QPM}^2}{c\varepsilon_0 n_{\omega}^2 n_{2\omega} \lambda_{\omega}^2 A_{eff}} \tag{3}$$

where P_{2w} is the SH output power of 532 nm, L is the efficient guided length and $P_{\omega}{}^{in}$ is the incident fundamental power at 1064 nm. A_{eff} is the nonlinear interaction area. A SH power of 14.87 mW could be generated for an incident fundamental power of 744 mW. The maximum normalized conversion efficiency of 3.55%/(W·cm^2) is achieved in a 11 mm long waveguide with periodically poled length of 8.7 mm. which is more than five times higher than the result published in the recent work [45]. Since the overlapping between the fundamental and SHG waves determines the conversion efficiency, we calculate the nonlinear interaction area through the following equation:

$$A_{eff} = \frac{\left[\iint |E_{\omega}(x,y)|^2 dxdy\right]^2 \iint |E_{2\omega}(x,y)|^2 dxdy}{\left[\iint E_{2\omega}(x,y) E_{\omega}^2(x,y) dxdy\right]^2} \tag{4}$$

where ω and 2ω represent the fundamental and SHG waves, respectively. The calculated value of No. 5 waveguide is about 387 μm^2, means a predicted conversion efficiency of 5.2%/W/cm^2. The calculated interaction area here is much smaller than our previous value of 917 μm^2 in ref 45. It also explain the promoted conversion efficiency in the present waveguide. The mode profile of SHG wave depicted in Fig. 4(b) show a diameter of 20 μm (1/e^2 intensity). The mode profile of fundamental wave in Fig. 4(c) seems like an inclined ellipse. The measured major and minor axes (1/e^2 intensity) of fundamental mode are estimated to be 22 μm and 13 μm, respectively. It should also be noted that the mode profiles in Figs. 4(b) and (c) did not fill the whole cladding area and keep away from the tracks. Therefor the scattering loss induced by the laser written tracks could be alleviated during the light propagation.

Optics EXPRESS

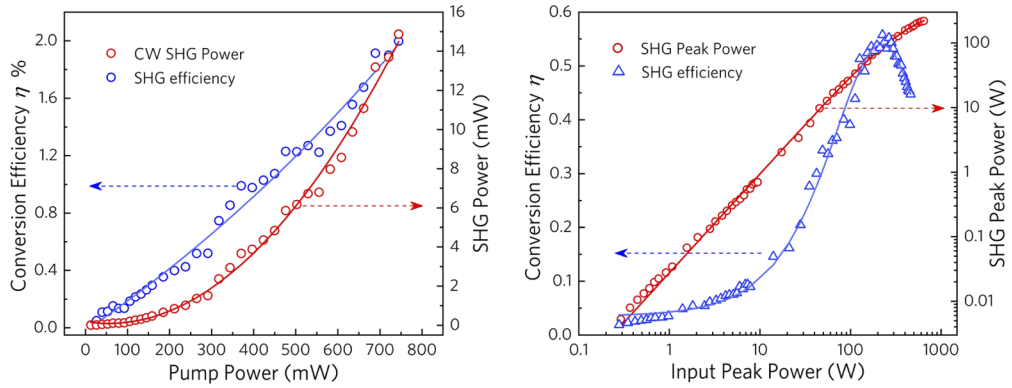

Fig. 6. Measured second harmonic output power and corresponding conversion efficiency as a function of the incident fundamental power of waveguide No. 5 at CW laser regime (a) and pulsed laser regime (b).

We have also investigated the SHG properties of the waveguide No. 5 by a Q-switched short pulse laser, which is shown in Fig. 6(b). For the low power regime, a normalized conversion efficiency of 3.81%/(W·cm^2) is achieved. The maximum conversion efficiency ($P_{2\omega}/P_{\omega}$) of 54.3% is achieved, in which 153 W SH peak power is obtained for an incident peak power of 282 W. We maintain the peak power at 1064 for several hrs. The conversion efficiency is stable. M. Triplett *et al.* reported the broadening of the SHG spectrum when pumping the PPSLT waveguide with high power CW light [44]. It is believed that the heating effect and the related temperature gradient inside the waveguide cross section are responsible for that. In our present pulse case, the peak power of the pump is high enough to excite a high power conversion efficiency. However, the average power is still very low due to the short pulse duration (3.6 ns), which greatly alleviate the heating effect during the SHG process. As indicated in Fig. 6(b), when the pump peak power increase further, the conversion efficiency decreased due to the down conversion from the SH to the fundamental wave [25]. The SHG characterization of all the waveguides in CW and shorter pulse regime are listed in Table 2. The conversion efficiencies of SH wave in pulsed regime listed in Table. 2 were measured while maintaining the input peak power smaller than 1W.

Table 2. The nonlinear SHG waveguides properties

Waveguides	Poling period (μm)	SH properties in CW regime		SH properties in pulse regime	
		Maximum SH power (mW)	Norm. efficiency%/(W·cm^2)	Norm. efficiency%/(W·cm^2) (low power)	Maximum $P_{2\omega}/P_{\omega}$
No.1	7.83	11.56	3.12	3.27	45.6%
No.2	7.85	12.59	3.25	2.71	47.1%
No.3	7.87	10.51	3.28	3.49	55.2%
No.4	7.89	11.69	3.39	3.69	49.6%
No.5	7.91	14.87	3.55	3.81	54.3%
No.6	7.93	8.33	2.17	2.35	32.5%
No.7	7.95	11.01	2.64	2.87	37.8%

Optics EXPRESS

4. Summary

In conclusion, we have demonstrated the fabrication of cladding waveguides in fan-out MgO doped fan-out PPSLT crystal by direct femtosecond laser writing. Seven low-loss individual waveguides are successfully fabricated with stepwise changed poling periods. The minimum insertion loss of the cladding waveguides is about 0.54 dB at wavelength of 1064 nm. In addition, we have investigated the SHG properties of all the seven waveguides in CW and short pulse regime with low average power. In the CW regime, the maximum normalized conversion efficiency is about 3.55%/(W·cm^2) of waveguides with 7.91 μm poling period in a periodically poled length of 8.7 mm. In the pulsed laser regime, a maximum conversion efficiency ($P_{2\omega}/P_{\omega}$) of 54.3% is achieved in an incident peak power of 282 W without any crystal damage induced by photorefractive. The above results indicate that MgO-doped PPSLT is a promising alternative to PPLN for the nonlinear optical photonic devices especially in the pulse/high power density domain, where the resistance to optical damage is the key requirements.

Funding

National Natural Science Foundation of China (11874239, 61775120, 91850110); Consejería de Educación, Junta de Castilla y León (SA046U16); Ministerio de Economía y Competitividad (FIS2013-44174-P, FIS2015-71933-REDT).

Disclosures

The authors declare no conflicts of interest.

References

1. I. Dolev, A. G. Padowicz, O. Gayer, A. Arie, J. Mangin, and G. Gadret, "Linear and nonlinear optical properties of MgO:LiTaO$_3$," Appl. Phys. B **96**(2), 423–432 (2009).
2. A. Bruner and D. Eger, "Second-harmonic generation of green light in periodically poled stoichiometric LiTaO$_3$ doped with MgO," Appl. Phys. Lett. **96**(12), 7445–7449 (2004).
3. P. Hu, L. Zhang, J. Xiong, J. Yin, C. Zhao, X. He, and Y. Hang, "Optical properties of MgO doped near-stoichiometric LiTaO$_3$ single crystals," Opt. Mater. **33**(11), 1677–1680 (2011).
4. S. Kim, Venkatraman Gopalan, K. Kitamura, and Y. Furukawa, "Domain reversal and nonstoichiometry in lithium tantalite," J. Appl. Phys. **90**(6), 2949–2963 (2001).
5. A. G. Getman, S. V. Popov, and J. R. Taylor, "7 W average power, high-beam-quality green generation in MgO-doped stoichiometric periodically poled lithium tantalate," Appl. Phys. Lett. **85**(15), 3026–3028 (2004).
6. D. S. Hum, R. K. Route, and M. M. Fejer, "Quasi-phase-matched second-harmonic generation of 532 nm radiation in 25°-rotated, *x*-cut, near-stoichiometric, lithium tantalate fabricated by vapor transport equilibration," Opt. Lett. **32**(8), 961–964 (2007).
7. F. Brunner, E. Innerhofer, S. V. Marchese, T. Südmeyer, R. Paschotta, T. Usami, H. Ito, S. Kurimura, K. Kitamura, G. Arisholm, and U. Keller, "Powerful red-green-blue laser source pumped with a mode-locked thin disk laser," Opt. Lett. **29**(16), 1921–1923 (2004).
8. S.-Y. Tu, A. H. Kung, Z. D. Gao, and S. N. Zhu, "Efficient periodically poled stoichiometric lithium tantalate optical parametric oscillator for the visible to near-infrared region," Opt. Lett. **30**(18), 2451–2453 (2005).
9. J. D. Rowley, S. Yang, and F. Ganikhanov, "Power and tuning characteristics of a broadly tunable femtosecond optical parametric oscillator based on periodically poled stoichiometric lithium tantalite," J. Opt. Soc. Am. B **28**(5), 1026–1036 (2011).
10. X. P. Hu, P. Xu, and S. N. Zhu, "Engineered quasi-phase-matching for laser techniques [Invited]," Photonics Res. **1**(4), 171–185 (2013).
11. Y. Ishigame, T. Suhara, and H. Nishihara, "LiNbO$_3$ waveguide second-harmonic-generation device phase matched with a fan-out domain-inverted grating," Opt. Lett. **16**(6), 375–377 (1991).
12. J.-P. Meyn and M. M. Fejer, "Tunable ultraviolet radiation by second-harmonic generation in periodically poled lithium tantalate," Opt. Lett. **22**(16), 1214–1216 (1997).
13. T. Hatanaka, K. Nakamura, and T. Taniuchi, "Quasi-phase-matched optical parametric oscillation with periodically poled stoichiometric LiTaO$_3$," Opt. Lett. **25**(9), 651–653 (2000).
14. J. Zimmermann, J. Struckmeier, and M. R. Hofmann, "Tunable blue laser based on intracavity frequency doubling with a fan-structured periodically poled LiTaO$_3$ crystal," Opt. Lett. **27**(8), 604–606 (2002).

Optics EXPRESS

15. N. E. Yu, M.-K. Oh, H. Kang, C. Jung, B. H. Kim, K.-S. Lee, D.-K. Ko, S. Takekawa, and K. Kitamura, "Continuous tuning of a narrow-band terahertz wave in periodically poled stoichiometric $LiTaO_3$ crystal with a fan-out grating structure," Appl. Phys. Express **7**(1), 012101 (2014).
16. D. Kip, "Photorefractive waveguides in oxide crystals: Fabrication, properties, and applications," Appl. Phys. B: Lasers Opt. **67**(2), 131–150 (1998).
17. J. Burghoff, S. Nolte, and A. Tünnermann, "Origins of waveguiding in femtosecond laser-structured $LiNbO_3$," Appl. Phys. A **89**(1), 127–132 (2007).
18. S. Gross and M. J. Withford, "Ultrafast-laser-inscribed 3D integrated photonics: challenges and emerging applications," Nanophotonics **4**(3), 323–352 (2015).
19. H. Tang, X.-F. Lin, Z. Feng, J.-Y. Chen, J. Gao, K. Sun, C.-Y. Wang, P.-C. Lai, X.-Y. Xu, Y. Wang, L.-F. Qiao, A.-L. Yang, and X.-M. Jin, "Experimental two-dimensional quantum walk on a photonic chip," Sci. Adv. **4**(5), eaat3174 (2018).
20. E. Kifle, P. Loiko, C. Romero, J. R. Vázquez de Aldana, A. Ródenas, V. Jambunathan, V. Zakharov, A. Veniaminov, A. Lucianetti, T. Mocek, M. Aguiló, F. Díaz, U. Griebner, V. Petrov, and X. Mateos, "Fs-laser-written erbium-doped double tungstate waveguide laser," Opt. Express **26**(23), 30826–30836 (2018).
21. Z. Huang, C. Tu, S. Zhang, Y. Li, F. Lu, Y. Fan, and E. Li, "Femtosecond second-harmonic generation in periodically poled lithium niobate waveguides written by femtosecond laser pulses," Opt. Lett. **35**(6), 877–879 (2010).
22. Y. L. Lee, N. E. Yu, C. Jung, and B.-A. Yu, "Second-harmonic generation in periodically poled lithium niobate waveguides fabricated by femtosecond laser pulses," Appl. Phys. Lett. **89**(17), 171103 (2006).
23. J. Thomas, M. Heinrich, J. Burghoff, and S. Nolte, "Femtosecond laser-written quasi-phase-matched waveguides in lithium niobate," Appl. Phys. Lett. **91**(15), 151108 (2007).
24. R. Osellame, M. Lobino, N. Chiodo, M. Marangoni, G. Cerullo, and R. Ramponi, "Femtosecond laser writing of waveguides in periodically poled lithium niobate preserving the nonlinear coefficient," Appl. Phys. Lett. **90**(24), 241107 (2007).
25. J. Burghoff, C. Grebing, S. Nolte, and A. Tünnermann, "Efficient frequency doubling in femtosecond laser-written waveguides in lithium niobate," Appl. Phys. Lett. **89**(8), 081108 (2006).
26. M. Marangoni, R. Osellame, R. Ramponi, S. Takekawa, M. Nakamura, and K. Kitamura, "Reverse-proton-exchange in stoichiometric lithium tantalate," Opt. Express **12**(12), 2754–2761 (2004).
27. T. Oka and T. Suhara, "Annealed proton-exchanged waveguide quasi-phase-matched second-harmonic generation devices in 8mol% MgO-doped congruent $LiTaO_3$ crystal," Jpn. J. Appl. Phys. **54**(10), 100304 (2015).
28. K. Sugioka and Y. Cheng, "Ultrafast lasers—Reliable tools for advanced materials processing," Light: Sci. Appl. **3**(4), e149 (2014).
29. R. R. Gattass and E. Mazur, "Femtosecond laser micromachining in transparent materials," Nat. Photonics **2**(4), 219–225 (2008).
30. T. Meany, M. Gräfe, R. Heilmann, A. Perez-Leija, S. Gross, M. J. Steel, M. J. Withford, and A. Szameit, "Laser written circuits for quantum photonics," Laser Photonics Rev. **9**(4), 363–384 (2015).
31. Y. L. Zhang, Q. D. Chen, H. Xia, and H. B. Sun, "Designable 3D nanofabrication by femtosecond laser direct writing," Nano Today **5**(5), 435–448 (2010).
32. D. Wei, C. Wang, H. Wang, X. Hu, D. Wei, X. Fang, Y. Zhang, D. Wu, Y. Hu, J. Li, S. Zhu, and M. Xiao, "Experimental demonstration of a three dimensional lithium niobate nonlinear photonic crystal," Nat. Photonics **12**(10), 596–600 (2018).
33. A. Ródenas, M. Gu, G. Corrielli, P. Paiè, S. John, A. K. Kar, and R. Osellame, "Three-dimensional femtosecond laser nanolithography of crystals," Nat. Photonics **13**(2), 105–109 (2019).
34. K. Sugioka, J. Xu, D. Wu, Y. Hanada, Z. Wang, Y. Cheng, and K. Midorikawa, "Femtosecond laser 3D micromachining: a powerful tool for the fabrication of microfluidic, optofluidic, and electrofluidic devices based on glass," Lab Chip **14**(18), 3447–3458 (2014).
35. K. M. Davis, K. Miura, N. Sugimoto, and K. Hirao, "Writing waveguides in glass with a femtosecond laser," Opt. Lett. **21**(21), 1729–1731 (1996).
36. F. Chen and J. R. Vázquez de Aldana, "Optical waveguides in crystalline dielectric materials produced by femtosecond-laser micromachining," Laser Photonics Rev. **8**(2), 251–275 (2014).
37. C. Cheng, Y. Jia, J. R. Vázquez de Aldana, Y. Tan, and F. Chen, "Hybrid waveguiding structure in $LiTaO_3$ crystal fabricated by direct femtosecond laser writing," Opt. Mater. **51**, 190–193 (2016).
38. L. Li, W. Nie, Z. Li, B. Zhang, L. Wang, P. Haro-González, D. Jaque, J. R. Vázquez de Aldana, and F. Chen, "Femtosecond Laser Writing of Optical Waveguides by Self-Induced Multiple Refocusing in $LiTaO_3$ Crystal," J. Lightwave Technol. **37**(14), 3452–3458 (2019).
39. A. Rodenas and A. K. Kar, "High-contrast step-index waveguides in borate nonlinear laser crystals by 3D laser writing," Opt. Express **19**(18), 17820–17833 (2011).
40. C. Cheng, C. Romero, J. R. Vázquez de Aldana, and F. Chen, "Superficial waveguide splitters fabricated by femtosecond laser writing of $LiTaO_3$ crystal," Opt. Eng. **54**(6), 067113 (2015).
41. W. Nie, C. Cheng, Y. Jia, C. Romero, J. R. Vázquez de Aldana, and F. Chen, "Dual-wavelength waveguide lasers at 1064 and 1079 nm in Nd:YAP crystal by direct femtosecond laser writing," Opt. Lett. **40**(10), 2437–2440 (2015).
42. F. Thorburn, A. Lancaster, S. McDaniel, G. Cook, and A. K Kar, "5.9 GHz graphene based Q-switched modelocked mid-infrared monolithic waveguide laser," Opt. Express **25**(21), 26166–26174 (2017).

Optics EXPRESS

43. G. Salamu, F. Jipa, M. Zamfirescu, and N. Pavel, "Cladding waveguides realized in Nd:YAG ceramic by direct femtosecond-laser writing with a helical movement technique," Opt. Mater. Express **4**(4), 790–797 (2014).
44. M. Triplett, J. Khaydarov, X. Xu, A. Marandi, G. Imeshev, J. Arntsen, A. Ninan, G. Miller, and C. Langrock, "Multi-watt, broadband second-harmonic-generation in MgO:PPSLT waveguides fabricated with femtosecond laser micromachining," Opt. Express **27**(15), 21102–21115 (2019).
45. L. Wang, X. Zhang, L. Li, Q. Lu, C. Romero, J. R. Vázquez de Aldana, and F. Chen, "Second harmonic generation of femtosecond laser written depressed cladding waveguides in periodically poled MgO:$LiTaO_3$ crystal," Opt. Express **27**(3), 2101–2111 (2019).